Efficiency Improvement Scheme for PV Emulator Based on a Physical Equivalent PV-Cell Model

HABES ALI KHAWALDEH[1,2], **(Graduate Student Member, IEEE),**
MOHAMMAD AL-SOEIDAT[1], **(Student Member, IEEE),**
MAJID FARHANGI[1], **(Student Member, IEEE),**
DYLAN DAH-CHUAN LU[1], **(Senior Member, IEEE),**
AND LI LI[1], **(Member, IEEE)**

[1]Faculty of Engineering and Information Technology, School of Electrical and Data Engineering, University of Technology Sydney, Ultimo, NSW 2007, Australia
[2]Department of Renewable and Sustainable Energy Engineering, Al al-Bayt University, Mafraq 25113, Jordan

Corresponding author: Habes Ali Khawaldeh (habes.a.khawaldeh@student.uts.edu.au)

ABSTRACT Recently, a photovoltaic (PV) emulator is proposed which is based on a combination of a constant current source and a one-diode photovoltaic model. Its superior dynamic performance is compatible with that of a real PV system. Although it is power efficient at the maximum power point (MPP), it suffers from high power loss around and at the open-circuit voltage (OCV) operation condition. The PV emulator can be used for PV system analysis and testing, such as maximum power point tracking (MPPT). This paper presents a new switching circuit which is placed in parallel with the diode string to minimize the power loss. The switching circuit consists of a two-switch non-inverting buck-boost DC/DC converter. When the operating point of the PV emulator moves from the current source region to the voltage source region, the converter, which is more efficient, switches in to replace the diode string seamlessly to maintain the circuit operation of the emulator. Experimental results show that in the worst case scenario, i.e. OCV condition, the efficiency and temperature of the proposed solution reach 81.47% and 30.1 °C respectively, as compared with 2.8% and 94.2 °C respectively for the diode string only case. In terms of dynamic response, the proposed PV emulator lags the real PV panel by only 3.5 ms as compared with 120 ms by a commercial emulator under the 30% to 60% insolation change test.

INDEX TERMS PV emulator, DC/DC converter, one-diode model, control system.

I. INTRODUCTION

Owing to the rapid increase in research and development in renewable energy systems in recent decades and the intermittent nature of most renewable energy sources, energy emulators become a critical tool to assist in the development and testing of these energy systems. A PV emulator is a power conditioning system, which is used to emulate the static and dynamic behaviors of the real solar cell, panel, or array [1]–[3]. The majority of existing PV emulators as reported in the literature are based on switching mode power supply (SMPS) topologies such as the buck, boost, and buck-boost converters due to their higher efficiency

than linear regulators [3]–[6]. The switching converter based approach is reliable and ideal for steady-state operation, but the controller bandwidth restricts its dynamic response. Hence, the converters are usually slower than a real PV panel [7], [8].

Different approaches compared with converter-based PV emulators have been reported [9]–[12]. In [9], a PV emulator based on a two-switch DC/DC buck-boost converter is proposed. The simulator uses a piecewise linear approach to derive the *I-V* curves and a low-cost 8-bit microcontroller to drive the converter to realize the PV electrical characteristics. In [10], the authors implemented a dual-diode PV model for the PV emulator, which requires two microprocessors. The prototype reduced the power and voltage errors to below 2% compared with the measured PV data. The authors in [11]

The associate editor coordinating the review of this manuscript and approving it for publication was Zhehan Yi .

presented a DC/DC-based PV emulator consisting of a step-up synchronous boost converter and a step-down synchronous buck converter. A dual current mode controller is used to provide a quick and precise replication of the *I-V* characteristics of the module. The power loss in this converter is lower than the conventional converter; however, the synchronous converter requires a more complex controller.

The authors of [3], [6], and [13], implemented a single-diode PV model for the PV emulator. It consists of a DC current source in parallel with a power diode string and some resistors. Based on the similarities of the electro-thermal behavior between the p-n junction diodes and a real PV panel, this design approach has a strong potential to improve the dynamic and stable performance, which was not verified in [13]. Furthermore, the ability and usefulness of the PV simulator based on the PV equivalent circuit model have not been thoroughly explored, such as the parametric extraction of actual PV panel for diode modeling, thermal behavior and adjustment of equivalent circuit model to mimic various operating conditions. The authors in [14] proposed a PV emulator based on transistors instead of diodes. For example, a 24-cell PV module can be emulated by three transistors. The transistor method reduces the component count, it has a high-power loss issue; the same issue that the diode method faces. Many MPPT methods have been presented and used in recent years, such as perturb and observe (P&O), fraction open-circuit voltage (FOCV), fraction short-circuit current (FSCC), incremental conductance (InC), hill climbing (HC) [15]–[17].

The main problem of the PV emulator using the physical equivalent single diode PV-cell is the thermal behavior, where the diode or transistor string temperature increases rapidly with increasing current rate [3], [13], [14]. In other words, the single diode module has a high power efficiency at the maximum power point because most of the current flows mainly to the output instead of the diode or transistor string. However, the emulator suffers from high power loss beyond the MPP, i.e. voltage source region, and the power loss reaches the highest in the open-circuit condition where all current flows to the diode or transistor string.

Even at high temperatures, the diodes or transistors are still functional but the output voltage (V_{PV}) will be decreased with respect to time based on the power diodes or transistors characteristic at high operating temperature also the lifetime of a power semiconductor device if it runs on high temperature is less than as compared with a low temperature operation condition [18], [19]. This issue is raised and studied in [3], but a solution is yet to provide. This paper, therefore, proposes a new switching circuit, which consists of a non-inverting buck-boost (NIBB) DC/DC converter and is inserted in parallel with the power semiconductor string (diodes are chosen for this study) to avoid the high temperature of the diode string when it is working at voltage source region, to minimize the aforementioned power loss while retaining the fast dynamics of the physically equivalent PV cell model, and to keep the operating temperature at an acceptable value

where the output voltage value keep constant with respect to time at each load value. Nevertheless, the total initial cost a little bit increases but the total running cost for the proposed solution is less than compared with the design based on the diode string only. In addition, a boost DC/DC converter loaded with a perturbing and observe (P&O) method is used to test and evaluate the proposed PV emulator [20], [21].

The paper is organized as follows. System overview and description of the proposed PV emulator is presented in Section II. Section III illustrates the design example of the proposed PV emulator. The experimental results and discussion are presented in Section IV. Finally, Section V concludes the paper.

II. SYSTEM OVERVIEW
A. OPERATION PRINCIPLE OF THE PV EMULATOR
The PV panel has two operating regions, as shown in Fig. 1. The first operation region, where the output voltage is less than the voltage at MPP. In this region the PV panel works as a current source, where the relationship between current and voltage is almost linear when the voltage increases from the voltage at the short circuit current (0V) to the voltage around the MPP. The diode string of the PV emulator will shape this portion of the *I-V* curve naturally (see the red dash box in Fig. 2). For the voltage source area, which defines as the operating point from the MPP towards the open-circuit voltage, the proposed switching circuit (Blue dash box in Fig. 2) will be operating in place of the diode string to minimize the power loss on the diode while achieving good PV emulator performance, as shown in Section IV.
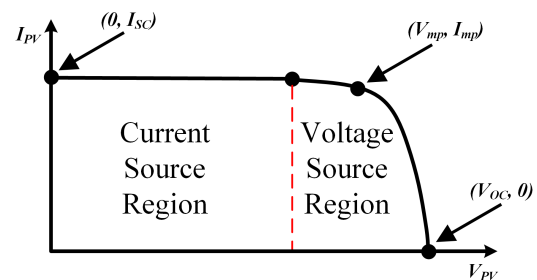

FIGURE 1. The characteristic *I-V* curve of the PV panel.

B. DESCRIPTION OF THE PROPOSED PV EMULATOR
For the sake of simplicity but acceptable accuracy, a PV emulator based on the physical single-diode PV model is used in this study as shown in Fig. 2 [3], [15], [22]–[24]. It consists of a DC input source, operating in constant current source mode, (I_{ph}), a string of diodes inserted in parallel with the NIBB DC/DC converter with a wide output voltage range for shaping the current/voltage curves of the selected PV source in the voltage source region, a TI-TMS320F28379D controller for sensing and controlling the output voltage (V_{PV}) and current (i_{PV}), computation and dispatch of duty cycle command, a MOSFET gate driver, and a pair of series and parallel resistors. Output load R_o changes based on the
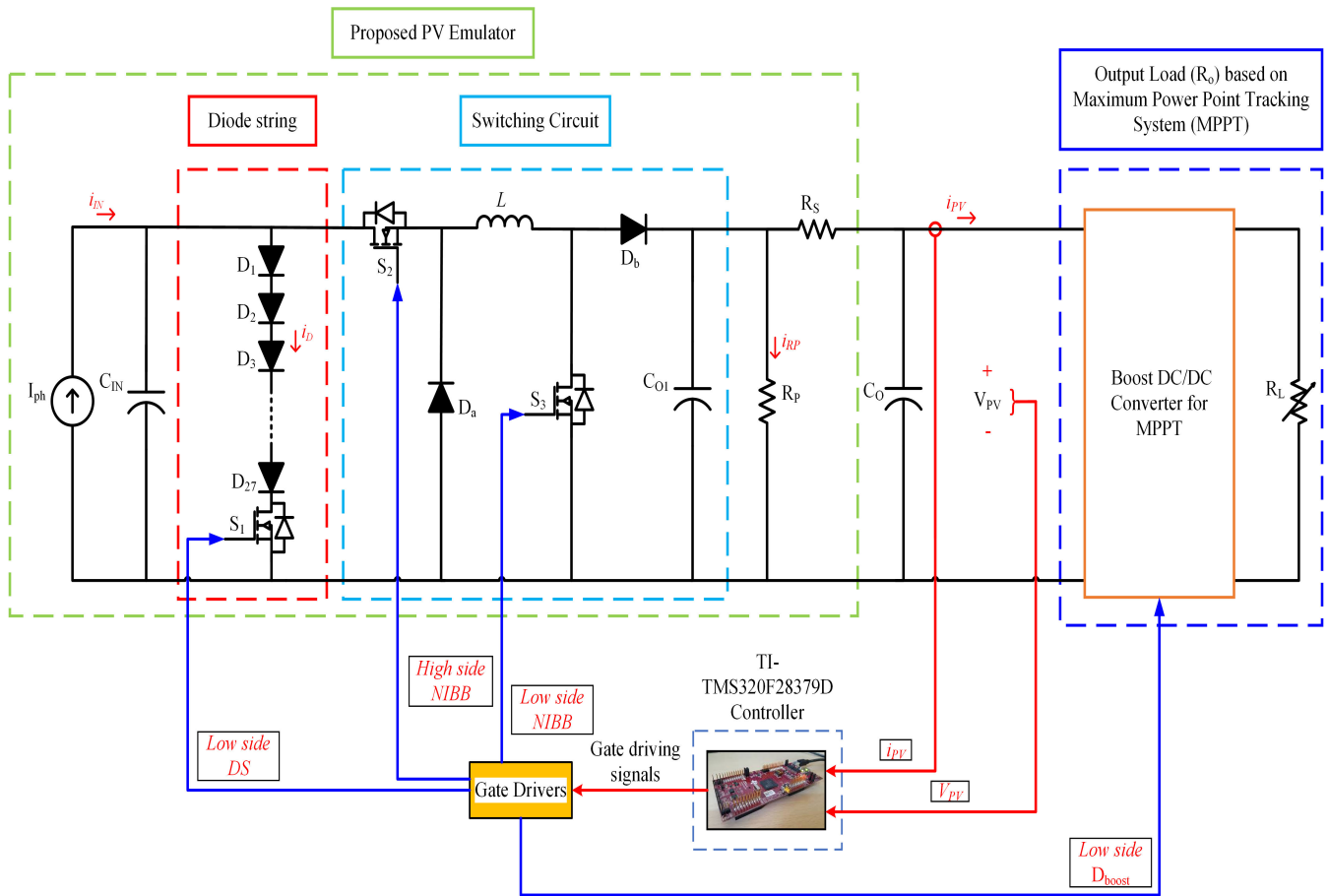
FIGURE 2. Block diagram of the proposed PV emulator and control scheme with boost DC/DC converter for MPPT system. A NIBB DC/DC converter is paralleled with the diode string to improve overall thermal performance.

MPPT system using boost DC/DC converter to test the performance of the PV emulator including both steady-state and dynamic behaviours, where a variable electronic load (Model: BK8500), is used as R_L.

III. DESIGN EXAMPLE OF THE PROPOSED PV EMULATOR
A. DESIGN OF THE DIODE STRING
The diode string design is studied deeply in [3]. Basically, it includes using the PV model equations, which considers ($Rseq$, $Rpeq$, N, and I_{ph}), to design the circuit parameters of the PV emulator to mimic a selected PV panel (Model: Powertech-ZM0954). The design challenge is how to extract real PV parameters, and solve the thermal issue of the PV emulator based on the physical single-diode PV model.

B. DC/DC CONVERTER SELECTION AND DESIGN
The second part of the PV emulator is the proposed switching circuit which is a switching power converter as shown in Fig. 2. The selection criteria for the paralleled DC/DC converter are in terms of simplicity, effectiveness and the ability to sweep through the entire voltage range of the selected PV panel. In order to mimic a low power PV system (<100 W), converter topologies such as buck, boost,

buck-boost and non-inverting buck-boost converter can be used [25]–[28]. The NIBB DC/DC converter is chosen for this work because of its voltage step-up and step-down capability. It can also work with a lower input voltage less than the OCV of the real PV panel, which reduces the device power stress. Moreover, it simplifies the hardware design due to its common ground feature. The NIBB DC/DC converter consists of two power MOSFETs S_2 and S_3, two diodes D_a and D_b, and an inductor L, as shown in Fig. 2. The inductor L is chosen to keep the converter operating in continuous conduction mode (CCM) to reduce the conduction losses. A $\pm 10\%$ maximum current ripple in the inductor is selected, at 100 kHz switching frequency, and the minimum inductance L_{min} is calculated as shown in (1) [9], [28].

$$L_{min} = \frac{D \times V_{in}}{f_s \times \Delta I} \qquad (1)$$

where the V_{in} is the maximum input voltage coming from the external DC power supply and it equals V_{oc}+forward voltage of the active components (diode and switch), where these values are constant, D is the duty cycle of the power switches, f_s is the switching frequency and ΔI is the maximum current ripple.

Table 1 shows the key parameters of the chosen PV panel (Model: Powertech-ZM9054), where the maximum OCV is 21.5V and the minimum short-circuit voltage is 0V. Two different input DC voltage source ranges are used to feed the proposed PV emulator circuit in this study, the first one when the maximum input voltage is less than OCV (19V), where the NIBB works in buck/boost mode, and the second one when the maximum input voltage is greater than the OCV (23V), where the NIBB works only in buck mode. The output PV emulator voltage based on NIBB converter varies from 17 to 21.5V, where the hysteresis output voltage control is applied for the converter.

The minimum critical inductance is chosen when the input source is at 23V and 0.65A. By setting the maximum duty cycle at 0.5 and using (1), L_{min} is 575μH. The inductor value is chosen as 1mH to keep the converter in CCM and reduce the current ripple. In order to provide at least 15V for both floating and non-floating gate drive for the MOSFETs S_2 and S_3, both low and high-side drivers are used. In this work TC4428 is used as a low side driver for switches S_1 & S_3, and IR2184PBF as a high side driver for switch S_2. The components used in this design are selected as shown in Table 2, based on the datasheet of the selected PV panel (as seen in Table 1) and the NIBB component power stress.

TABLE 1. Specifications of the selected PV panel.

POWERTECH	
Model	ZM9054
Maximum Power (P_{max})	10W($\pm$5%)
Open Circuit Voltage (V_{oc})	21.5V
Short Circuit Current (I_{sc})	0.65A
Rated Voltage (V_{mp})	17.5V
Rated Current (I_{mp})	0.57A
Maximum System Voltage	1000V
Test Condition	AM1.5, 1000 $\frac{W}{m^2}$, 25C^o

TABLE 2. Components details of the proposed PV emulator.

Component	Model/Value
Digital Controller	TMS320F28379D
Switching Frequency	100 kHz
MOSFET	IRF540N
MOSFET Driver for S_1 & S_3	TC4428
MOSFET Driver for S_2	IR2184PBF
D_a & D_b	MBR2035CT
D_1,......D_{27} (Diode String)	1N5400
Current Sensoer	LEM-LTS-6-NP
L (Boost Converter)	1mH
L (NIBB Converter)	1mH
Programmable PV Emulator Device	EA-PSI 9360-15
Programmable DC Electronic Load	BK8500

C. OPERATION PRINCIPLE OF THE PROPOSED PV EMULATOR

The proposed topology has two operating modes as shown in Fig. 3. The first mode occurs when the output voltage of the proposed PV emulator is less than the voltage at the MPP (i.e., current source region). In this mode, S_1 & S_2 are ON, where majority of the current flows through the output and a fraction to the diode string to shape the desired *I-V* curve during this region. The NIBB converter is disabled. The second mode occurs when the NIBB DC/DC converter starts to operate once the voltage reaches the MPP and operates beyond this point toward the OCV (i.e., voltage-source region). Both S_2 and S_3 are ON to charge the inductor (Fig. 3 (b)). Then both switches are OFF to discharge the inductor through D_a and D_b (Fig. 3 (c)). By controlling the duty cycle of the MOSFETs based on the variation of the output resistive load, the output voltage will be shaped according to the characteristic of the selected PV panel. The diode string is not engaged in this mode to reduce power loss.
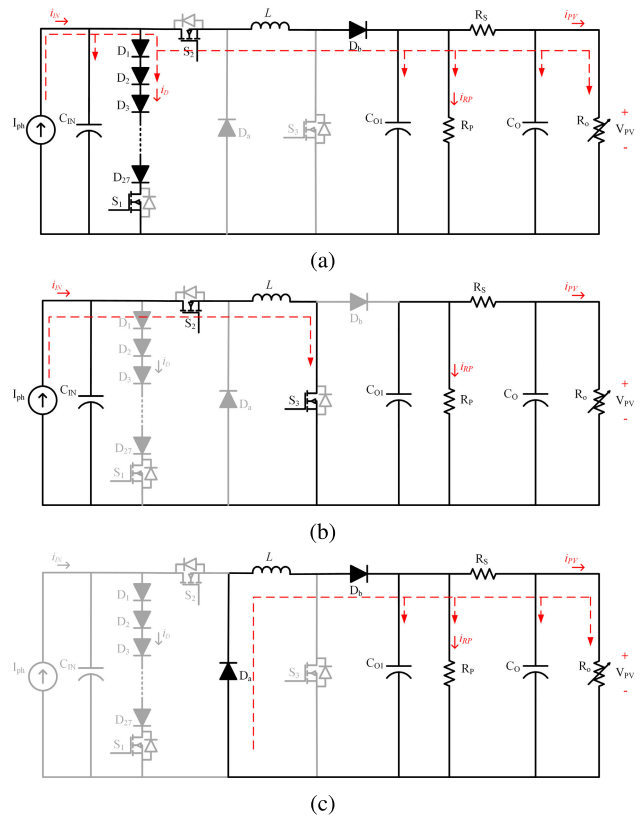

FIGURE 3. Operation principle of the proposed PV emulator typology: (a) mode I when the S_1 & S_2 are ON, and (b) & (c) mode II when NIBB works.

D. CONTROLLER AND CONTROL STRATEGY

The microcontroller used in this work is the LAUNCHXL-F28379D from TI [29], [30]. The closed-loop control system and MPPT algorithm are implemented based on the control block diagram as shown in Fig. 4 and the mode selection algorithm is designed based on the control flow chart shown in Fig. 5. The program starts with specifying the symbols for the duty cycles D_1, D_2, D_3, and D_{boost} for S_1, S_2, S_3,

and S_{boost}, respectively. since the initial current sensor output value may not be precisely zero due to the residual magnetization in the current sensor used (Model: LEM-LTS-6-NP). An initial zero calibration has to be performed by measuring the I_{PV} value and set it as a reference to cancel this offset. Suppose V_{PV} is less than 16.5V. In that case, the PV emulator works in the linear operation region (the relationship between current and voltage almost linear before maximum power point) or diode string mode, where S_1 and S_2 are ON, S_3 is OFF. After that, the output voltage (V_{PV}) is measured. If V_{PV} is still less than 16.5V, the emulator remains in the same mode (i.e. Mode I). On the other hand, if V_{PV} is larger than 16.5V and smaller than 17.5V, the controller will wait for 1ms and recheck the V_{PV} status to decide if mode changing is needed. The voltage range from 16.5V to 17.5V, a 1V window, is used as the hysteresis band control. Lastly, if V_{PV} is larger than 17.5V and less than 21.5V (OCV for the selected PV panel), that means the PV emulator has now entered the voltage source region or NIBB DC/DC converter mode. S_1 is turned OFF, and NIBB begins to operate (S_2 and S_3 shared the same control signal). The control strategy used in Mode II is based on the Look-up table (LUT) and curve fitting [31], [32]. These two methods are popular control methods used to implement I-V curves of real PV panels using power electronics converters [9], [33]. A boost DC/DC converter with a P&O algorithm is used to test the proposed PV emulator at different irradiation levels, where the experimental results are shown in Fig. 13.
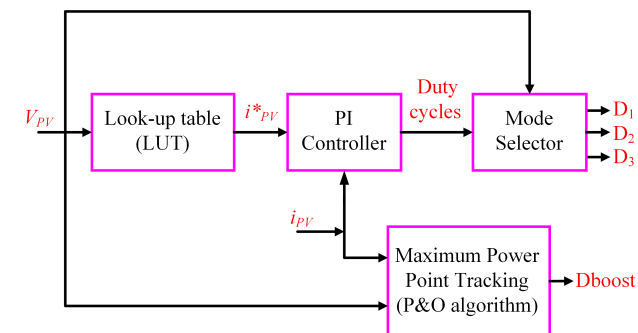

FIGURE 5. Flowchart of the operating mode selection algorithm.

FIGURE 6. Experimental setup for the proposed PV emulator.

FIGURE 4. Block diagram of the closed-loop control.

IV. EXPERIMENTAL RESULTS AND DISCUSSION

A hardware prototype is built and tested in the laboratory as shown in Fig. 6. The maximum OCV (V_{oc}) is 21.5V and the short-circuit current (I_{sc}) is 0.65A. The performance of the proposed close-loop PV emulator is compared with both the real PV panel and a commercial programmable PV emulator (PPVE, model: EA-PSI 9360-15 2U). The experimental results show matching electrical characteristics among the proposed emulator, the selected PV panel and the commercial PV emulator.

Fig. 7 shows the measured steady-state results for the proposed PV emulator in Mode I where only the diode string is
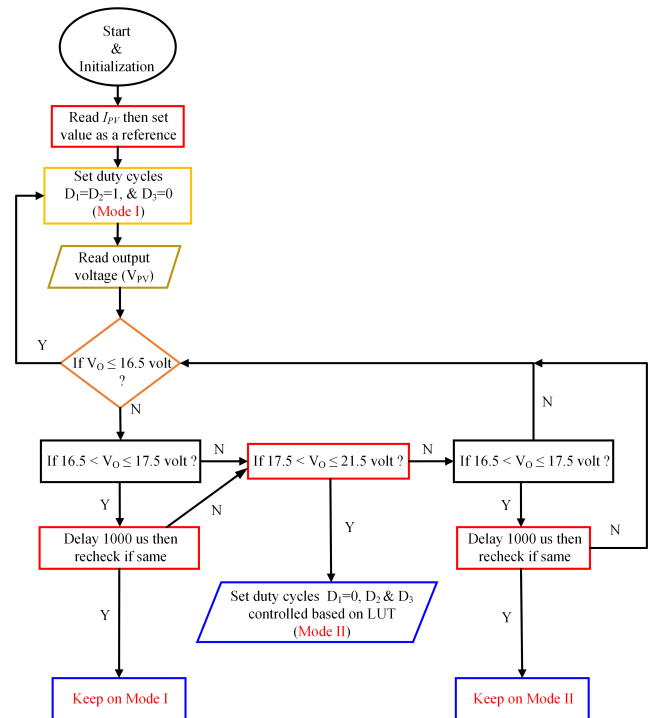
active. The top waveform shows the gate control signal for S_1, followed by the control signal for S_2, then the control signal for S_3 & output voltage, when the output load is at 4.7Ω, and 22Ω, respectively. It is clear from the figure that S_1 & S_2 are ON, and S_3 is OFF.

There are two control scenarios based on the input voltage DC source value as mentioned above. The first one is when a 23V DC input source is used, where the NIBB converter works as a buck converter in Mode II, as shown in Fig. 8. Based on the figure, it is notable that the duty cycle value of the S_2, and S_3 is less than 0.5 at OCV. In the second control scenario, a 19V DC input source is used as a DC
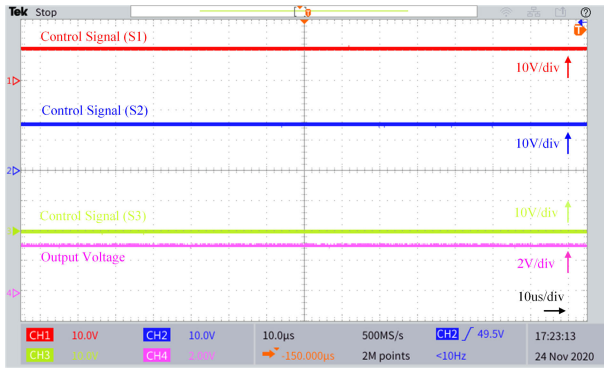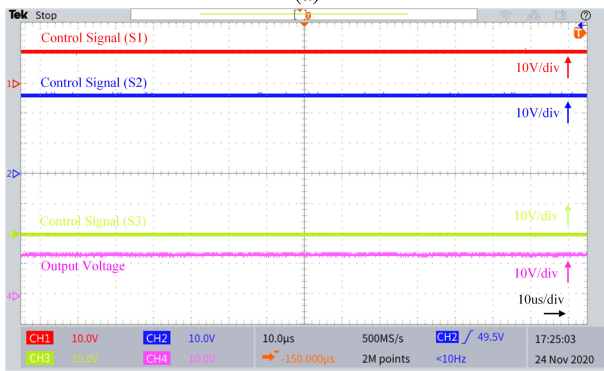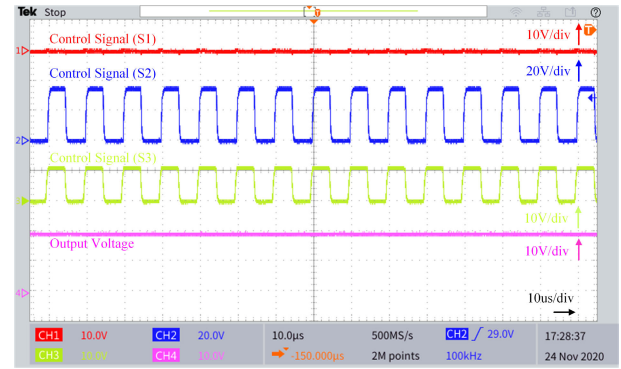
FIGURE 7. The gate control signals, and output voltage of the proposed PV emulator: (a) at 4.7Ω, and (b) at 22Ω resistive load. Time base: 10us/div. Ch1(red): 10V/div. Ch2(blue): 10V/div. Ch3(green): 10V/div. Ch4(a-pink): 2V/div. Ch4(b-pink): 10V/div. Diode string mode (First control scenario).

FIGURE 8. The PWM control signals, and output voltage of the proposed PV emulator: (a) at 47Ω, and (b) at 270Ω resistive load. Time base: 10us/div. Ch1(red): 10V/div. Ch2(blue): 20V/div. Ch3(green): 10V/div. Ch4(pink): 10V/div. Non-inverting buck-boost mode (First control scenario).
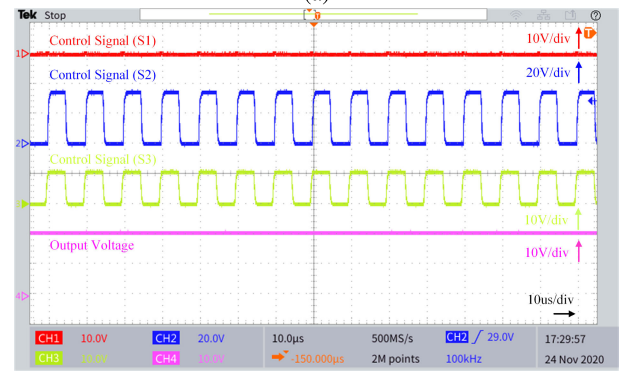
supply, where the NIBB converter works as a boost converter in Mode II, as shown in Fig. 9. Notably, the duty cycle value of the S_2, and S_3 is greater than 0.5. However, the boost mode control scenario is used for the efficiency and dynamic evaluation.

The experimental steady-state results for the proposed PV emulator in Mode II, based on the first and second control scenarios, where only the NIBB DC/DC converter is active, are shown in Figs. 8 and 9, respectively. The top waveform presents the PWM control signal for S_1, followed by the control signal for S_2, then the control signal for S_3 & output voltage of the proposed PV emulator, when the output load is at 47Ω, and 270Ω, respectively. It is clear that the NIBB converter is operating, where the S_2 & S_3 are switching, and S_1 is OFF.

Fig. 10 shows the dynamic behavior of the proposed PV emulator when the operating mode changes between Mode I and Mode II based on the output load variation. V_{PV} equals 13.5V and 18.7V when the load is at 22Ω and 47Ω, respectively. In Mode I, where the only diode string is working, as shown in Fig. 10, it is clear that the diode string operates, where the S_1 and S_2 are ON, and the S_3 is OFF. In Mode II, where the NIBB DC/DC converter is active, it is shown that the NIBB converter operates, where the S_2 and S_3 are switching based on the sharing PWM and S_1

is OFF. Notably, the proposed emulator can switch between the modes smoothly, where the output power equals 8.28W (at 13.5V & 0.614A) in Mode I, and 7.44W (at 18.7V & 0.398A) in Mode II in this example.

Figs. 11 and 12 show a comparison between the *I-V* and *P-V* characteristic curves based on experiment and simulation results for the commercial programmable PV emulator device (PPVE, model: EA-PSI 9360-15 2U), proposed PV emulator (PVE), PVE MATLAB simulation, and the actual PV panel (Model: Powertech-ZM0954). Fig. 11 (a) shows the *I-V* curve and Fig. 11 (b) shows the *P-V* curve for the same setup. From the Fig. 11, it is clear that the actual PV panel short circuit current (I_{sc}) equal to 0.65A and the OCV equals 21.5V at 990W/m^2, and 26°C. To simulate the same electrical characteristic, the DC power source, works at constant current mode, is limited to the 0.65A based on (2) and the voltage set at 23V or 19V based on the control scenario. The real PV panel current and voltage measured again at another irradiation level (795W/m^2 at 26.5°C), where the short circuit current drops to 0.52A, and the OCV reduces to 21.3V. The current and voltage values are used as input for the PV emulator, where the DC power source, is limited to the 0.52A based on (2) and the voltage set at 23V or 19V based on the control scenario. The *I-V* and *P-V* curves for the commercial PPVE, PVE MATLAB
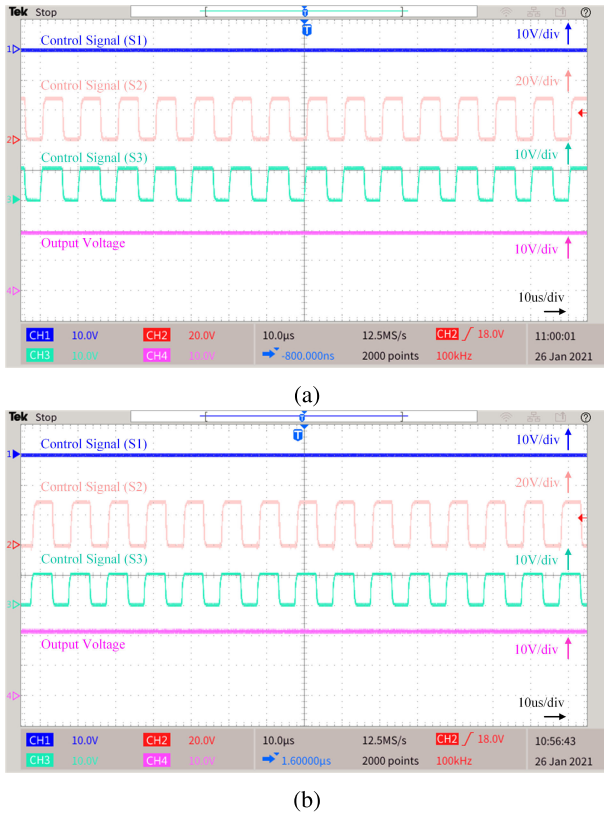
(a)

(b)

FIGURE 9. The PWM control signals, and output voltage of the proposed PV emulator: (a) at 47Ω, and (b) at 270Ω resistive load. Time base: 10us/div. Ch1(blue): 10V/div. Ch2(red): 20V/div. Ch3(green): 10V/div. Ch4(pink): 10V/div. Non-inverting buck-boost mode (Second control scenario).

FIGURE 10. The PWM control signals for S_1, S_2 and S_3, respectively, and output voltage of proposed PV emulator when operation mode changed. Time base: 4s/div. Ch1(red): 10V/div. Ch2(blue): 20V/div. Ch3(green): 10V/div. Ch4(pink): 10V/div.

simulation, proposed PV emulator, and actual PV panel are plotting in Fig. 12. The enhanced PV emulator shows high performance, where the current and voltage match the one generated from commercial PPVE and the actual PV panel.
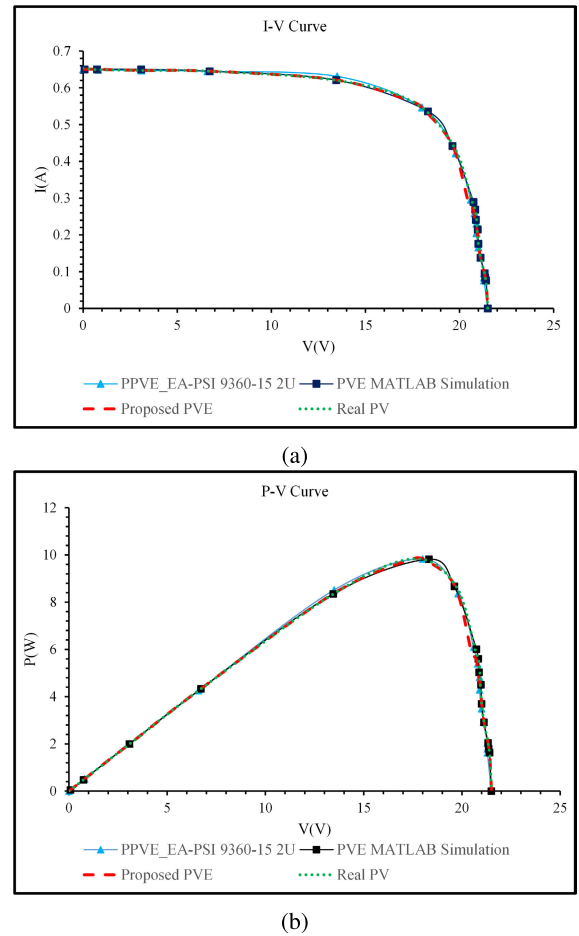

(a)

(b)

FIGURE 11. The comparison of characteristic curves of the real photovoltaic panel, proposed PV emulator (PVE) and commercial PV emulator device at $I_{sc} = 0.65A$ and $V_{oc} = 21.5V$: (a) *I-V* curve, and (b) *P-V* curve.

The current density of the photovoltaic panel (I_{ph}) is linearly proportional to the solar radiation and is also affected by the temperature according to the mathematical equation given by [7], [22]:

$$I_{ph} = (I_{ph,n} + K_I \triangle T)\frac{G}{G_n} \qquad (2)$$

where $I_{ph,n}$ is the light-generated current at the standard test condition (STC), and $\triangle T$ is the temperature variation, and it can be defined by (3), K_I is the PV cells short circuit current temperature coefficient, G $[\frac{W}{m^2}]$ is the irradiation density at the PV cell surface and G_n is the irradiation at STC.

$$\triangle T = T - T_n \qquad (3)$$

where T and T_n the actual and temperatures at STC [K], respectively.

MPPT test has been conducted to validate and evaluate the proposed PV emulator at different irradiation levels. Figs. 13 (a) and (b) presents the *I-V* curve drawing by changing the duty cycle of the boost DC/DC converter (D_{boost}) from 10% to 90%. The experimental setup is shown in Fig. 6. The MPP at different irradiation levels have been shown in Figs. 13 (d) and (e), respectively, by using the MPPT
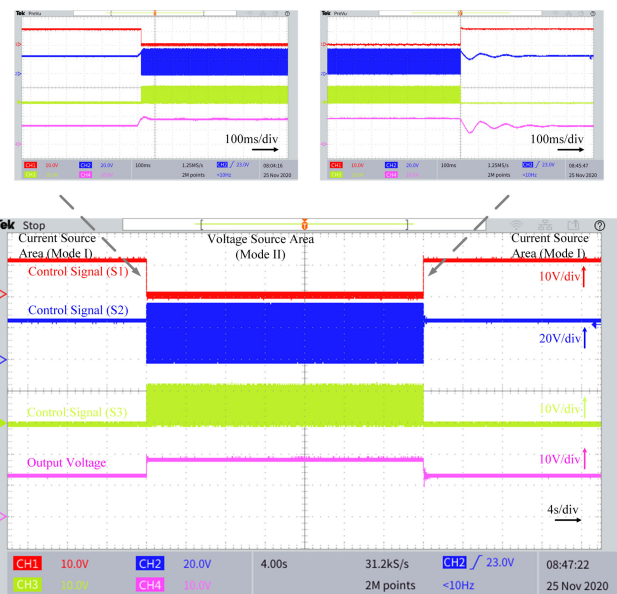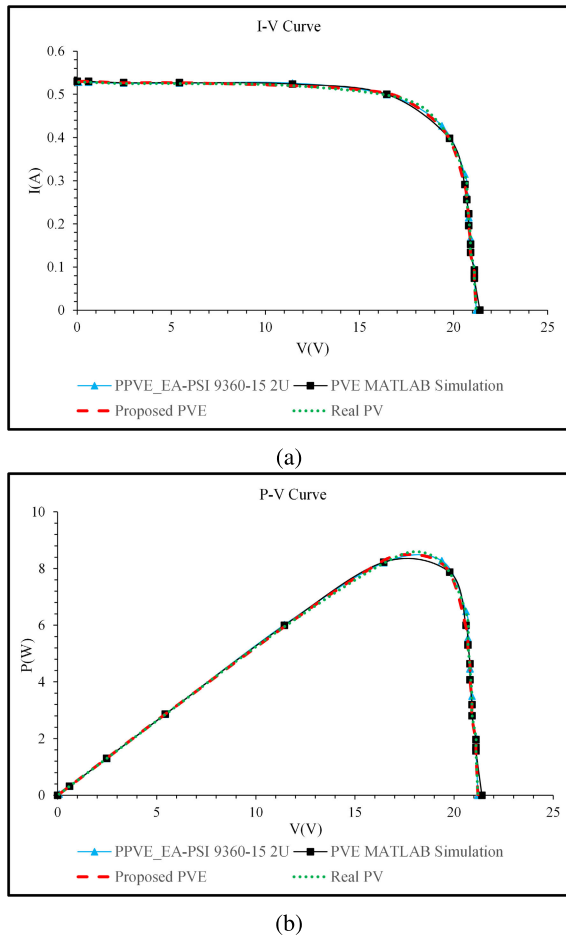
(a)

(b)

FIGURE 12. The comparison of characteristic curves of the real photovoltaic panel, proposed PV emulator (PVE) and commercial PV emulator device at I_{SC} = 0.52A and V_{OC} = 21.3V: (a) *I-V* curve, and (b) *P-V* curve.

method (P & O). Figs. 13 (c) and (f) shows the *I-V* and *P-V* curves for the actual PV system and the proposed PV emulator under two various irradiation levels, where the performance of the proposed emulator shown an identical behavior compared with the real PV system. It is notable from Fig. 13 (f) that the PV emulator will have two MPPs (Points A, and B). The voltage and current at the first MPP (point A) equal 17.4V and 0.562A, respectively. Where the voltage and current at the second MPP (point B) equal 17.3V and 0.485A, respectively. Also, from the figure, it is clear that, the performance of the proposed PV emulator is not affected by the used MPPT system. To sum up, the tracking system is able to track the MPPs at the same irradiation levels, where the tracked current and voltage match up with the one in Fig. 13 (f).

Fig. 14 shows a comparison of power loss between the PV emulator built by using diode string and the proposed PV emulator that has both diode string and NIBB converter. Thermal imaging camera (FLIR TG 167) is used to show the change of temperature against the output current. It can be seen that the diode string temperature increases from 29.5°C to 94.2°C, which indicates the rapid increase in the power loss. After using the proposed switching circuit,

the temperature only increases from 27.5°C to 35.1°C on the diode string in Mode I. In Mode II, the diode string is switched OFF, the diode string temperature drops back to the room temperature. Meanwhile, the NIBB DC/DC converter begins to work in this mode. The temperature increases from 24.8°C to a maximum of 30.1°C in the NIBB branch. It is also shown in Fig. 14 that the power efficiency of the PV emulator based on diode string decreases from 98.8 % to 2.8% at the output loads of 10Ω and 270Ω, respectively. In addition, the emulator based on both diode string and NIBB converter shows significant improvement in overall conversion efficiency, where the efficiency varies from 98.8 % to 81.48% using the same experiment setup.

The mean time to failure (MTTF) concept of a device is used to compare the PV emulator based on diode string and the proposed approach [18], [19]. The lifetime of the PV emulator based on the diode string approach at the worst-case scenario, open-circuit voltage (OCV) operation condition, where the operating temperature equals 94.2°C is 15000 hours compared with the 147000 hours lifetime of the PV emulator based on the proposed platform where the maximum operating temperature equal to 30.1°C.

The power loss analysis for the PV emulator based on diode string compared with the proposed topology is shown in Fig. 15. It is clear from the figure that the power loss for the emulator design using only diode string increases rapidly especially at the voltage source region, where it reaches the maximum power dissipation at the OCV operation condition. In addition, the proposed topology shows a good behavior compared to the diode string solution in terms of power loss. However, this comparison can be used to explain the increase in cost for the presented solution.

The dynamic response of the powertech PV panel (ZM9054), proposed PV emulator and programmable PV emulator device (PPVE, model: EA-PSI 9360-15 2U) are shown in Fig. 16, where I_{PV} varied from 0.185A to 0.385A according to the programmable electronic load (Model: BK8500). From Fig. 16 (a), the proposed PV emulator shows a dynamic response lags by 3.5ms with respect to the real PV panel. Nevertheless, the programmable PV emulator lags by 120ms with respect to the real PV panel, as shown in Fig. 16 (b). The dynamic response of the proposed PV emulator also compared with some of the existing PV emulator platforms, as shown in Table 3. The proposed emulator shows the best response time compare with the existing solutions.

V. CONCLUSION

This paper presents the design and implementation of a PV emulator based on a switching circuit in parallel with a diode string to minimize the power loss and improve the thermal performance of the emulator. The switching circuit consists of a two-switch NIBB DC/DC converter. The proposed PV emulator can mimic a PV panel with highly accurate results compared with both the real PV panel and commercial PV emulator under steady-state and dynamic operating conditions. System performance has been studied
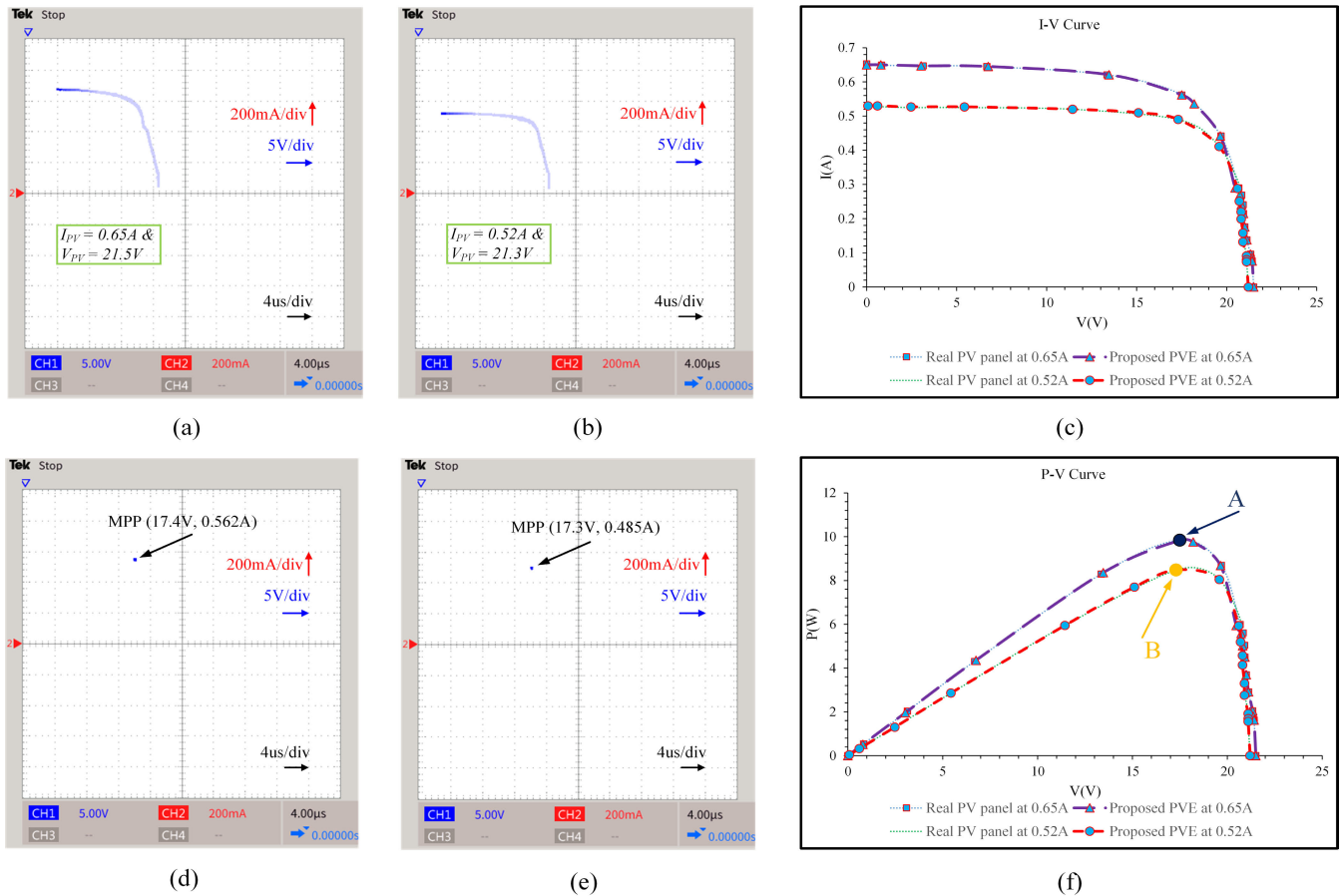
FIGURE 13. Experimental results showing the: (a & b) *I-V* curve drawing based on the MPPT (boost DC/DC converter), when the I_{PV} equals 0.65A (990W/m^2), and 0.52A (795W/m^2), respectively, (d & e) showing the MPP at the different irradiation levels, and (c & f) presenting the *I-V*, and *P-V* curves respectively.
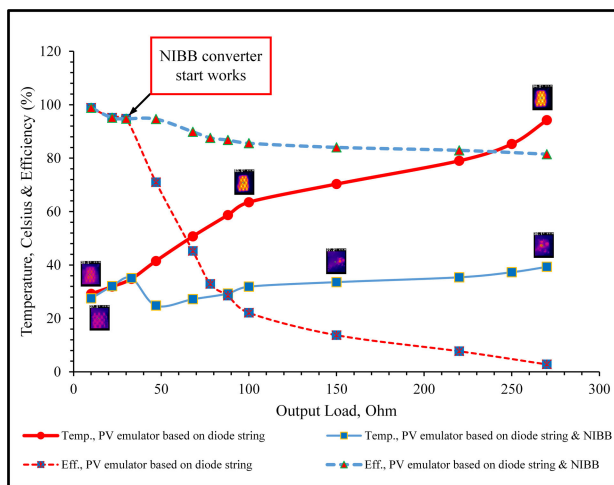

FIGURE 14. Thermal behaviour based on output load variation for PV emulator based on diode string and proposed PV emulator using both diode string and NIBB converter.
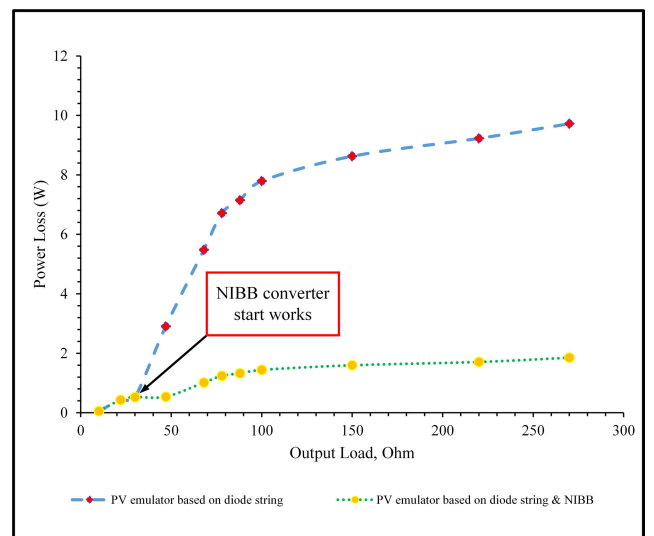

FIGURE 15. Power loss comparison between PV emulator based on diode string and proposed topology.

from both thermal and electrical perspectives. The main problem of the PV emulator based on the physical equivalent single-diode PV-cell module is the increase of diode string temperature, specifically at the open circuit condition (i.e., maximum power dissipation). The diode string temperature increases from 29.5°C to 94.2°C, from short-circuit

condition to open-circuit condition respectively with the absence of any cooling system, and the power efficiency decreases from 98.8 % to 2.8%. With the presence of NIBB converter, which starts to work in the voltage-source region of the PV emulator, the overall power efficiency improves

TABLE 3. Comparison from different aspect for existing platforms with the proposed PV emulator.

No.	Author\s (Ref.)	Converter used	Control complexity	Cost	Dynamic response (ms)
1	Cirrincione et al. [34]	Buck	Complex	Moderate	160
2	EA-PSI 9360-15 2U [35]	SMPSU	Complex	High	120
3	Ayop and Tan [22]	Buck	Complex	Moderate	21.25
4	Remache et al. [23]	Boost	Complex	High	18
5	Proposed PV emulator	Diode String & NIBB	Moderate	Moderate	3.5
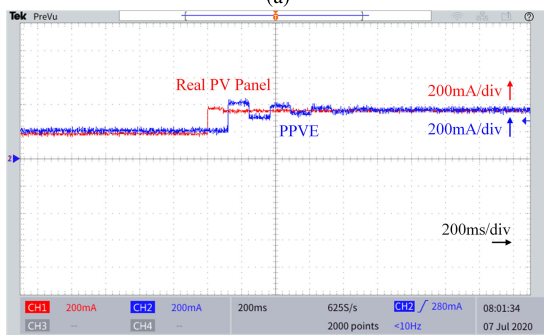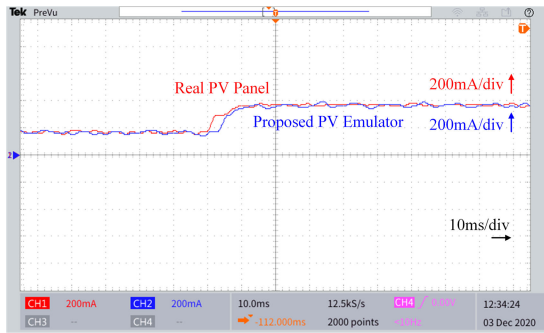
FIGURE 16. The dynamic PV characteristic when I_{SC} converted from 0.185A to 0.385A based on load variation: (a) Real PV panel compared with proposed PV emulator, and (b) Real PV panel compared with programmable PV emulator device. Time base (a): 10ms/div. Time base (b): 200ms/div and I_{SC}: 200mA/div.

and varies between 98.8% and 81.48% under the same operating condition. The dynamic response of the proposed PV emulator shows an improvement of 116.5ms compared to the commercial PV emulator device. Also, the proposed PV emulator has been tested and verified by using one of the well-known MPPT techniques (P&O), where the result was closed to the result when the actual PV system is used.

REFERENCES

[1] J. P. Ram, H. Manghani, D. S. Pillai, T. S. Babu, M. Miyatake, and N. Rajasekar, "Analysis on solar PV emulators: A review," *Renew. Sustain. Energy Rev.*, vol. 81, pp. 149–160, Jan. 2018.

[2] A. K. Panchal, "A per-unit-single-diode-model parameter extraction algorithm: A high-quality solution without reduced-dimensions search," *Sol. Energy*, vol. 207, pp. 1070–1077, Sep. 2020. [Online]. Available: http://www.sciencedirect.com/science/article/pii/S0038092X20307830

[3] H. A. Khawaldeh, H. Aljarajreh, M. Al-Soeidat, D. D.-C. Lu, and L. Li, "Performance investigation of a PV emulator using current source and diode string," in *Proc. 26th Int. Conf. Syst. Eng. (ICSEng)*, Dec. 2018, pp. 1–5.

[4] R. Ayop and C. W. Tan, "A comprehensive review on photovoltaic emulator," *Renew. Sustain. Energy Rev.*, vol. 80, pp. 430–452, Dec. 2017.

[5] C.-H. Chang, C.-A. Cheng, and H.-L. Cheng, "Modeling and design of the LLC resonant converter used as a solar-array simulator," *IEEE J. Emerg. Sel. Topics Power Electron.*, vol. 2, no. 4, pp. 833–841, Dec. 2014.

[6] H. A. Khawaldeh, M. Al-Soeidat, D. D. Lu, and L. Li, "Simple and fast dynamic photovoltaic emulator based on a physical equivalent PV-cell model," *J. Eng.*, vol. 2021, no. 5, pp. 276–285, May 2021. [Online]. Available: https://ietresearch.onlinelibrary.wiley.com/doi/abs/10.1049/tje2.12032

[7] N. Ullah, F. Nisar, and A. A. Alahmadi, "Closed loop control of photo voltaic emulator using fractional calculus," *IEEE Access*, vol. 8, pp. 28880–28887, 2020.

[8] D. Chariag and L. Sbita, "Design and simulation of photovoltaic emulator," in *Proc. Int. Conf. Green Energy Convers. Syst. (GECS)*, Mar. 2017, pp. 1–6.

[9] D. D. C. Lu and Q. N. Nguyen, "A photovoltaic panel emulator using a buck-boost DC/DC converter and a low cost micro-controller," *Sol. Energy*, vol. 86, no. 5, pp. 1477–1484, May 2012.

[10] S. M. H. Hosseini and A. A. Keymanesh, "Design and construction of photovoltaic simulator based on dual-diode model," *Sol. Energy*, vol. 137, pp. 594–607, Nov. 2016. [Online]. Available: http://www.sciencedirect.com/science/article/pii/S0038092X16303966

[11] W. Zhang and J. W. Kimball, "DC–DC converter based photovoltaic simulator with a double current mode controller," *IEEE Trans. Power Electron.*, vol. 33, no. 7, pp. 5860–5868, Jul. 2018.

[12] U. K. Shinde, S. G. Kadwane, R. K. Keshri, and S. Gawande, "Dual mode controller-based solar photovoltaic simulator for true PV characteristics," *Can. J. Electr. Comput. Eng.*, vol. 40, no. 3, pp. 237–245, 2017.

[13] M. Ünlü and S. Çamur, "A simple photovoltaic simulator based on a one-diode equivalent circuit model," in *Proc. 4th Int. Conf. Electr. Electron. Eng. (ICEEE)*, Apr. 2017, pp. 33–36.

[14] A. Zegaoui, M. Aillerie, P. Petit, and J.-P. Charles, "Universal transistor-based hardware SIMulator for real time simulation of photovoltaic generators," *Sol. Energy*, vol. 134, pp. 193–201, Sep. 2016.

[15] M. Azharuddin, T. S. Babu, N. Bilakanti, and N. Rajasekar, "A nearly accurate solar photovoltaic emulator using a dSPACE controller for real-time control," *Electr. Power Compon. Syst.*, vol. 44, no. 7, pp. 774–782, Apr. 2016.

[16] A. Ali, K. Almutairi, S. Padmanaban, V. Tirth, S. Algarni, K. Irshad, S. Islam, M. H. Zahir, M. Shafiullah, and M. Z. Malik, "Investigation of MPPT techniques under uniform and non-uniform solar irradiation condition—A retrospection," *IEEE Access*, vol. 8, pp. 127368–127392, 2020.

[17] S. H. Hanzaei, S. A. Gorji, and M. Ektesabi, "A scheme-based review of MPPT techniques with respect to input variables including solar irradiance and PV arrays' temperature," *IEEE Access*, vol. 8, pp. 182229–182239, 2020.

[18] X. Yang, B. Sun, Z. Wang, C. Qian, Y. Ren, D. Yang, and Q. Feng, "An alternative lifetime model for white light emitting diodes under thermal–electrical stresses," *Materials*, vol. 11, no. 5, p. 817, May 2018.

[19] H. Givi, E. Farjah, and T. Ghanbari, "A comprehensive monitoring system for online fault diagnosis and aging detection of non-isolated DC–DC converters' components," *IEEE Trans. Power Electron.*, vol. 34, no. 7, pp. 6858–6875, Jul. 2019.

[20] J.-E. Hernandez-Diez, C.-F. Mendez-Barrios, S.-I. Niculescu, and E. Barcenas-Barcenas, "A current sensorless delay–based control scheme for MPPT–boost converters in photovoltaic systems," *IEEE Access*, vol. 8, pp. 174449–174462, 2020.

[21] S. Padmanaban, N. Priyadarshi, J. B. Holm-Nielsen, M. S. Bhaskar, F. Azam, A. K. Sharma, and E. Hossain, "A novel modified sine-cosine optimized MPPT algorithm for grid integrated PV system under real operating conditions," *IEEE Access*, vol. 7, pp. 10467–10477, 2019.

[22] R. Ayop and C. W. Tan, "Rapid prototyping of photovoltaic emulator using buck converter based on fast convergence resistance feedback method," *IEEE Trans. Power Electron.*, vol. 34, no. 9, pp. 8715–8723, Sep. 2019.

[23] S. E. I. Remache, A. Y. Cherif, and K. Barra, "Optimal cascaded predictive control for photovoltaic systems: Application based on predictive emulator," *IET Renew. Power Gener.*, vol. 13, no. 15, pp. 2740–2751, Nov. 2019.

[24] M. Farahani, M. A. Shamsi-Nejad, and H. R. Najafi, "Design and construction of a digital solar array simulator with fast dynamics and high performance," *Sol. Energy*, vol. 196, pp. 319–326, Jan. 2020.

[25] D. G and S. N. Singh, "Selection of non-isolated DC–DC converters for solar photovoltaic system," *Renew. Sustain. Energy Rev.*, vol. 76, pp. 1230–1247, Sep. 2017.

[26] S. Sivakumar, M. J. Sathik, P. S. Manoj, and G. Sundararajan, "An assessment on performance of DC–DC converters for renewable energy applications," *Renew. Sustain. Energy Rev.*, vol. 58, pp. 1475–1485, May 2016.

[27] L. J. Jeremy, C. A. Ooi, and J. Teh, "Non-isolated conventional DC–DC converter comparison for a photovoltaic system: A review," *J. Renew. Sustain. Energy*, vol. 12, no. 1, Jan. 2020, Art. no. 013502.

[28] D.-H. Kim and B.-K. Lee, "An enhanced control algorithm for improving the light-load efficiency of noninverting synchronous buck–boost converters," *IEEE Trans. Power Electron.*, vol. 31, no. 5, pp. 3395–3399, May 2016.

[29] *TMS320F2837xD Dual-Core Delfino Microcontrollers*, Texas Instrum., Dallas, TX, USA, 2018.

[30] L. R. Merchan-Villalba, J. M. Lozano-Garcia, J. G. Avina-Cervantes, H. J. Estrada-Garcia, and J. Martinez-Patino, "Matrix converter based on SVD modulation using a microcontroller as unique controlling device," *IEEE Access*, vol. 7, pp. 164815–164824, 2019.

[31] L. Shen, F. Yang, X. Wang, and P. Comerford, "Functional curve fitting algorithm via multi-heterogeneous data curve," *IEEE Access*, vol. 5, pp. 470–479, 2017.

[32] J. Ren, "Digital predistorter for short-wave power amplifier with improving index accuracy of lookup table based on FPGA," *IEEE Access*, vol. 7, pp. 182881–182885, 2019.

[33] J. Sa, H. Gu, Y. An, Y. Luo, and Z. Zhang, "Study on curved surface fitting of countersink based on point cloud," *IEEE Access*, vol. 8, pp. 106464–106470, 2020.

[34] M. Cirrincione, M. C. Di Piazza, M. Pucci, and G. Vitale, "Real-time simulation of photovoltaic arrays by growing neural gas controlled DC–DC converter," in *Proc. IEEE Power Electron. Specialists Conf.*, Jun. 2008, pp. 2004–2010.

[35] *EA-PSI 9360-15 2U*, EA-Elektro-AutomatikGmbH, Viersen, Germany, May 2015.

HABES ALI KHAWALDEH (Graduate Student Member, IEEE) received the B.E. degree in electrical and computer engineering from The Hashemite University, Jordan, in 2009, and the M.S. degree in electrical power engineering from Yarmouk University, Jordan, in 2013. He is currently pursuing the Ph.D. degree in power electronics with the Faculty of Engineering and Information Technology, University of Technology Sydney (UTS), Australia. Since 2018, he has been a Casual Academician with UTS for various power electronics subjects. Since July 2009, he has been working as an electrical engineer with different companies in Jordan. He was a part-time Faculty Member with Yarmouk University for various power electronics subjects. He was a full-time Faculty Member with Al-Hussein Bin Talal University, from 2015 to 2018. His current research interests include renewable energy (RE) systems, power converter design for RE applications, battery systems, multi-port DC/DC converters, and energy conversion systems for the smart grid. He received a Grant from Al al-Bayt University for his Ph.D. degree. He is currently a reviewer for several IEEE, IET, and Elsevier journals.

MOHAMMAD AL-SOEIDAT (Student Member, IEEE) received the B.E. degree in electrical engineering from Al-Hussein Bin Talal University, Ma'an, Jordan, in 2013, with a focus on communication engineering, the M.E. degree in electrical engineering from The University of Sydney, Sydney, Australia, in 2016, and the Ph.D. degree in power electronics from the University of Technology Sydney (UTS), Sydney, in 2020. In 2013, he joined Zain Jordan as a Radio Access Network Engineer. His research interests include power electronics and energy conversion systems for the smart grid, renewable energy applications, and energy storage systems. He received a Grant from Al-Hussein Bin Talal University (AHU) for his master's and Ph.D. degrees.

MAJID FARHANGI (Student Member, IEEE) received the B.Sc. degree in electronics engineering from Islamic Azad University, Iran, in 2015, the M.Eng. degree in electrical engineering from The University of Sydney, Australia, in 2018. He is currently pursuing the Ph.D. degree in power electronics with the Faculty of Engineering and Information Technology, University of Technology Sydney (UTS), Australia. His main research interests include high-frequency DC-DC converters, high-frequency inverters, multilevel converters, and induction heating systems. He is a reviewer of several IEEE journals and conferences.
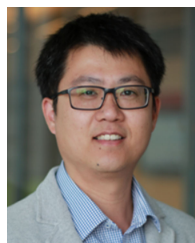
DYLAN DAH-CHUAN LU (Senior Member, IEEE) received the Ph.D. degree in electronic and information engineering from The Hong Kong Polytechnic University, Hong Kong, in 2004. In 2003, he joined PowerELab Ltd., as a Senior Design Engineer, where he was responsible for industrial switching power supply projects. He was a full-time Faculty Member with The University of Sydney, Australia, from 2006 to 2016, where he currently holds an honorary position. He joined the University of Technology Sydney, Australia, in July 2016. He is also a Professor and the Head of the Discipline of Electrical Power and Energy Systems, School of Electrical and Data Engineering. He has authored or coauthored more than 120 international journals and held two patents in power electronics. His current research interests include efficient, cost-effective, and reliable power conversion for renewable energy sources, energy storage systems, and microgrids. He is also serving as the Chair for the Joint Chapter IAS/IES/PELS (IEEE New South Wales Section) and an Associate Editor for the IEEE Transactions on Industrial Electronics.

LI LI (Member, IEEE) received the B.S. degree from the Huazhong University of Science and Technology, in 1996, the M.S. degree from Tsinghua University, in 1999, and the Ph.D. degree from the University of California, Los Angeles, in 2005. From 2005 to 2007, he was a Research Associate with the University of New South Wales at the Australian Defence Force Academy (UNSW@ADFA). From 2007 to 2011, he was a Researcher with National ICT Australia, Victoria Research Laboratory, Department of Electrical and Electronic Engineering, The University of Melbourne. In 2011, he joined UTS, where he is currently an Associate Professor. He held several visiting positions at the Beijing Institute of Technology, Tsinghua University, and UNSW@ADFA. His research interests include control theory and power system control. He is also serving as an Associate Editor of *IET Renewable Power Generation*.

● ● ●